Received: 26 March 2018 | Revised: 5 July 2018 | Accepted: 1 August 2018

DOI: 10.1111/jace.16012

SPECIAL ISSUE ARTICLE

Journal of the American Ceramic Society

# High-temperature stable inverse opal photonic crystals via mullite-sol-gel infiltration of direct photonic crystals

**Priscila Bueno**[1,2] | **Kaline Pagnan Furlan**[1] | **Dachamir Hotza**[2] | **Rolf Janssen**[1]

[1]Institute of Advanced Ceramics, Hamburg University of Technology, Hamburg, Germany

[2]Interdisciplinary Laboratory for the Development of Nanostructures (LINDEN), Federal University of Santa Catarina (UFSC), Florianópolis, Brazil

**Correspondence**
Rolf Janssen, Institute of Advanced Ceramics, Hamburg University of Technology, Hamburg, Germany.
Email: janssen@tuhh.de

**Funding information**
German Research Foundation (DFG), Grant/Award Number: SFB 986, "M3", project C5

**Abstract**

Three-dimensionally ordered macroporous materials for photonic or refractory applications have been developed by an innovative approach based on mullite sol-gel infiltration of direct photonic crystals followed by burn-out and calcination. Direct photonic crystals were obtained using polystyrene spheres templates either by vertical convective self-assembly or by drop casting. The samples were then infiltrated by spin coating with mullite sol-gels prepared with two different compositions (74 wt.% $Al_2O_3$, 26 wt.% $SiO_2$ and 80 wt.% $Al_2O_3$, 20 wt.% $SiO_2$). The inverse opal photonic crystals prepared with both sol-gels presented a highly ordered porosity and the high-alumina composition showed stability up to 1500°C. After inversion of the structure (polymeric template burn-out), the high-alumina composition showed roundness of the PS templated pores closer to an ideal sphere (Ø = 0.967) when compared to the low-alumina composition (Ø = 0.954). Although the inverse opal photonic crystals did not present a photonic bandgap, they showed structural stability at high temperatures, which enable their application as refractory materials.

**KEYWORDS**

high-temperature applications, infiltration, mullite sol-gel, photonic crystals

## 1 | INTRODUCTION

The development of new high-temperature stable 3D photonic crystals is currently a challenge, driven by its possible use in different systems, such as reflectors in solar cells,[1] solid oxide fuel cells (SOFCs), photocatalysts,[2] and new-generation photonic thermal barrier coatings (TBCs).[3] Particularly, the latter one requires an advanced thermal stability to operate at high temperatures while maintaining specific optical characteristics.[4,5]

Photonic crystals, also known as opaline structures, can exist in the form of direct photonic crystals[6] (thin films of colloidal particles) and inverse opal photonic crystals[7] (highly porous 3D structures). Direct photonic crystals are usually manufactured by vertical convective self-assembly,[8] in which monodisperse colloidal organic particles[9] such as polystyrene (PS) or poly (methyl methacrylate) (PMMA) are typically used. These structures can also be produced by spin coating[10,11] and drop casting.[12] Although the vertical convective self-assembly process usually leads to more homogeneous films, it is a time-consuming process (3-5 days depending on the conditions) when compared with drop casting, which can be performed in less than 30 minutes.[13]

Meanwhile, inverse opal photonic crystals are usually obtained by the infiltration of templates, such as the organic-based direct photonic crystals. This can be carried out by deposition methods, such as atomic layer deposition (ALD)[14] or chemical vapor deposition (CVD),[15] and also by vertical and horizontal infiltration of colloidal suspensions or sol-gels.[16] The latter are less time and energy consuming methods, when in comparison to ALD or CVD.

After infiltration, a heating or etching treatment is performed to remove the template, resulting in a three-dimensional highly ordered macroporous material (3-DOM). Thereby, the sol-gel infiltration synthesis route can be regarded as low cost and versatile considering the comprehensive knowledge of sol-gel formation. Moreover, the sol-gel infiltration can lead to high-performance materials when precursors with high purity are employed.

By means of sol-gel infiltration, a variety of ceramic oxide materials can be produced such as alumina,[17] zirconia,[18] titania,[19] and even ternary or quaternary oxides. Considering the latter one, mullite offers both advanced thermal properties and a well-established database of powder metallurgy as well as sol-gel synthesis.[20] Therefore, mullite matrix was chosen here as suitable demonstrator for 3DOMs based on ternary oxides. Mullite is mixture of $Al_2O_3$ and $SiO_2$ that exists in two different ratio compositions, 2:1 and 3:2.[21] Mullite has achieved outstanding importance as a material for both traditional and advanced ceramics because of its favorable thermal and mechanical properties.[22] Mullite products are therefore widely used in high-temperature applications. Moreover, the raw materials for its production (eg, alumina, silica, aluminum silicates, clays, among others) are widely found in nature. Nevertheless, specific mullite studies are not so widespread when comparing to titania or zirconia. Synthesis of mullite by sol-gel is well reported and can be tailored in a way that mullite forms already at temperatures as low as 1000°C.[23–25] However, a very strict control of the sol-gel and high-purity precursors are necessary to produce a sol-gel with low crystallization temperature for mullite (≤1000°C). In general, mullite sol-gel synthesis deal with phase segregation, forming a mixture of mullite and $\alpha$-alumina[26,27] associated with higher crystallization temperature (>1200°C).[28,29] Furthermore, the crystallization and segregation behavior of the mullite sol-gels is generally reported only for the sol-gel synthesis and characterization, but not for the behavior of such a sol-gel when in contact with different substrates and interfaces, as for example a polymeric template.

In this work, we demonstrate the synthesis of sol-gel-based mullite inverse opal photonic crystals by sol-gel infiltration via spin coating, as a low-cost and versatile technique to produce thermally stable inverse opal photonic crystals for high-temperature applications.

## 2 | MATERIALS AND METHODS

### 2.1 | Preparation of mullite gels

Mullite gels with two compositions, nearly stoichiometric low-alumina $3Al_2O_3{\cdot}2SiO_2$ (74 wt.% $Al_2O_3$, 26 wt.% $SiO_2$) and high-alumina content $5Al_2O_3{\cdot}2SiO_2$ (80 wt.% $Al_2O_3$, 20 wt.% $SiO_2$), were synthesized by sol-gel, based in a procedure reported elsewhere.[23–25] For the low-alumina gel, a 50 mL sol was prepared by mixing 1 mol/L aluminum nitrate nonahydrate (ANN, 99.997% trace metals basis, Sigma-Aldrich) prepared in a 50/50 vol.% water/ethanol with 50 vol.% tetraethyl orthosilicate (TEOS, ≥99.0%, Sigma-Aldrich) aqueous solution. The ratio of ANN to TEOS was calculated to result in mullite with 74 wt.% alumina and 26 wt.% silica. The high alumina content gel was prepared following the same procedure, here aiming at 80 wt.% alumina and 20 wt.% silica. For both compositions, the precursors were poured into a Teflon beaker, and mixed under continuous stirring at 60°C until the gel was formed. Since the gelation time is dependent on the hydrolysis rate, it was also dependent on the composition. A slow hydrolysis of 10-14 days was performed to obtain the gels. After gelation, the gels were dried in a heating chamber at 80°C for 24 hours and powdered for further investigation. For the infiltration, the gels were not dried, but diluted (see Horizontal Infiltration by Spin Coating topic).

### 2.2 | Template preparation

Monodisperse PS particles (Microparticles GmbH) with diameter of 721 ± 20 nm were assembled onto planar sapphire substrates (A-oriented 25 × 20 mm, Crystec GmbH). Prior to self-assembly, the substrates were cleaned by soaking for 1 hour in an ultrasonic bath using an alkaline detergent solution (Mucasol, Merz Hygiene), then brushed and washed with hot tap water followed by deionized water, and finally blow dried with filtered nitrogen. To further clean and make the surfaces more hydrophilic, a RF-oxygen plasma treatment (PolaronPT7160; Quorum Technologies Ltd, Laughton, UK) process was applied on the substrates for 20 minutes. For generating the templates, two different process were employed: vertical convective self-assembly[7–9] and drop casting.[12]

The vertical convective self-assembly experiments were carried out by diluting stock dispersions of PS particles with deionized filtered (Minisart NML, pore size 0.1 μm, Sartorius Stedim Biotech) water to 1 mg/mL into a 50 mL Teflon beaker, and subsequent homogenizing by a magnetic stirrer. The substrates were weighted and placed into the Teflon beakers that were later placed inside a heating chamber (VTR 5022, Heraeus Instruments, Hanau, Germany) at constant temperature of 60°C and left for at least 120 hours until the opaline film was formed. After that, the substrate was removed from the chamber and dried for 12 hours at room temperature. The excess of PS on the substrate backside was removed very carefully with the aid of a razor blade and ethanol. Substrates were weighed and

the height of the photonic crystals in the substrate was estimated.

For drop casting, a suspension of 3 mg/mL of PS particles was prepared by diluting the spheres in a 50 vol.% water/ethanol solution. The clean substrate was horizontally placed in a hot plate at 60°C, on which 150 μL of the suspension was dropped. Samples were left to dry for at least 30 minutes at 60°C to form the opaline film.

## 2.3 | Horizontal infiltration by spin coating

The mullite gel was removed from the Teflon beaker before complete hydrolysis, aiming for a low viscosity to allow the further infiltration. Furthermore, the gel was again diluted in 50/50 vol.% mixture of filtered deionized water and ethanol in order to minimize even more the viscosity. The substrates were placed horizontally in a spin coater (SPS Spin 150) and 150 μL of the diluted mullite gel was dropped on the top of the PS direct photonic crystals. The spin coating assisted infiltration was carried out at 500 $min^{-1}$ for 40 seconds. The infiltrated template was then removed from the spin coater and dried for 12 hours at room temperature. This procedure was performed twice for each template in order to allow full infiltration of the template (polystyrene direct photonic crystals). The inverse opal photonic crystals were then obtained by burnout of the PS particles in air at 500°C for 1 hour using heating and cooling rates of 0.8°C/min. The schematic of the production of the mullite inverse opal photonic crystals is summarized in Figure 1.

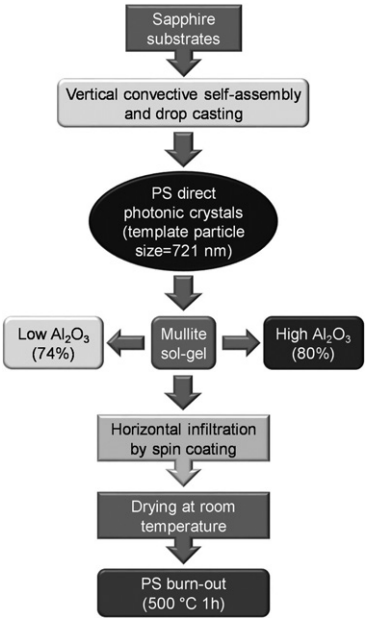


**FIGURE 1** Flowchart of the production of sol-gel-based mullite inverse opal photonic crystals

## 2.4 | Characterization

The particle size analysis was carried out via dynamic light scattering (Zeta Sizer, Malvern) using 1.65 as refractive index for the mullite sol. Six measurements were carried for each set. The mullite sol-gel was dried, powdered and annealed in a muffle furnace at temperatures of 900°C for 1 hour, 1000°C for 1 hour, and 1500°C for 8 hours with a heating rate of 5°C/min. Phase identification of dried and powdered gels was performed after annealing by X-ray diffraction analysis (XRD, Bruker D8 Advance) with Cu K$\alpha$ radiation, 40 kV, 40 mA, range 10°-70°, step size of 0.01°, and step time of 2 seconds.

The thermal stability of the mullite inverse opal photonic crystals was analyzed by heat treatments performed at 900, 1000, 1200°C for 1 hour, 1400°C for 4 hours, and 1500°C for 8 hours with a heating rate of 5°C/min. All treatments were performed using resistive furnaces (muffle and tubular) in air. The structural morphological changes caused by the heat treatments were assessed by scanning electron microscopy (SEM, Leo 1530 Gemini; Zeiss *Supra* 55 VP, Carl Zeiss).

A microstructural analysis of the PS direct photonic crystals and the mullite photonic crystals was carried out from digitalized binary images of SEM micrographs, as shown in Figure 2. Using an image analysis software (Image J, NIH, US), representative SEM micrographs with the same magnification were first converted into binary (black and white) images. The software then calculated the percentage area of space between PS microspheres (PS direct photonic crystals) and percentage area occupied by pores after burnout and heat treatment (mullite inverse opal photonic crystals). In this way, it was possible to estimate the minimum distance (interstitial space) between PS microspheres; and, after the inversion of structure with mullite sol-gel, the average strut thickness of cells. Besides that information, the software also provided the total area of PS microspheres and pores, which allowed calculating the mean diameter of PS microspheres and pores. A roundness parameter (defined by Equation 1) for both microspheres and pores, $\emptyset$, was also estimated using the scattering of the measured diameters. Thereby, it is assumed that a change from the ideal round starting spherical shape would not result in an ideal isotropic shrinkage (a swelling is not likely and can be therefore neglected). Instead, the change in pore/microsphere shape is controlled essentially by the coordination of the surrounding particles/grains, which is non-ideal in ALD synthesized structures.

$$\emptyset = 1 - d_{sd}/d_a \quad (1)$$

where $d_{sd}$ is the standard deviation of n diameter measures; $d_a$ is the average of n diameter measures, either of PS

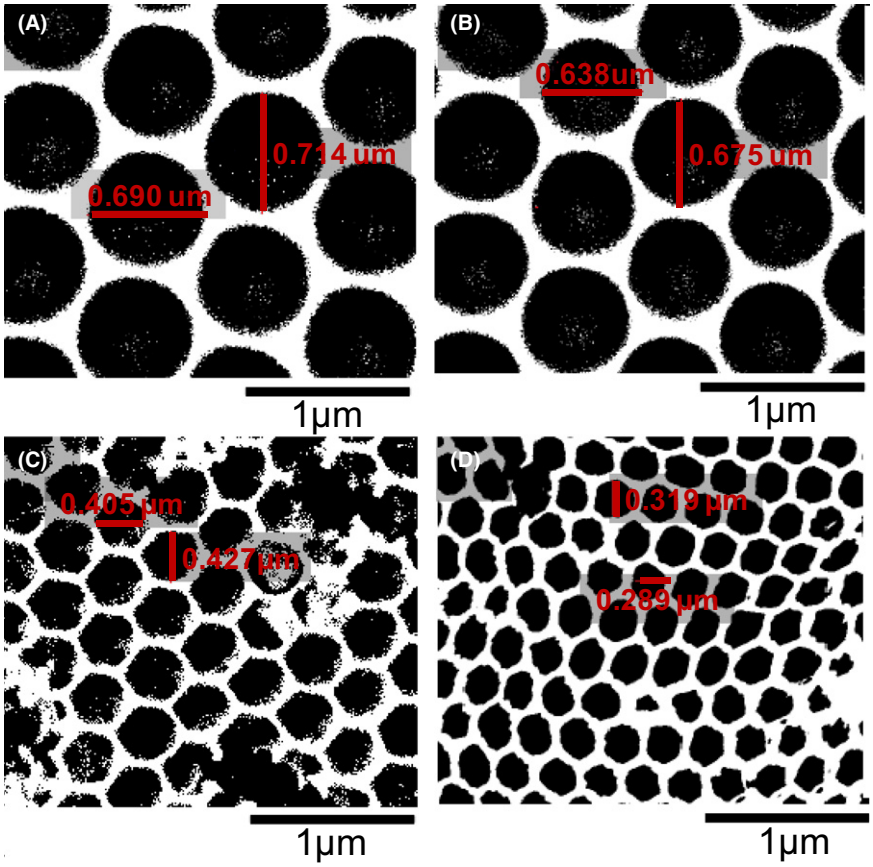


**FIGURE 2** Example of binary images of SEM micrographs of: (A) PS direct photonic crystals obtained by self-assembly; (B) PS direct photonic crystals obtained by drop casting; (C) mullite inverse opal photonic crystals infiltrated with low-alumina sol-gel annealed at 1200°C; and (D) mullite inverse opal photonic crystals infiltrated with high-alumina sol-gel annealed at 1500°C. Image analysis by Image J

microspheres or pores, respectively, before or after thermal treatment.

Annealed samples were also subjected to grazing incidence X-ray diffraction analysis (GI-XRD, Bruker D8 Advance) with Cu K$\alpha$, 40 kV, 40 mA, range 10°-60°, step size 0.01°, step time of 2 seconds, and incident angle of 1.5°.

## 3 | RESULTS AND DISCUSSION

The average particle size of the gels obtained by DLS was 117 nm for the sol-gel with 74 wt.% $Al_2O_3$ and 258 nm for the gel with 80 wt.% $Al_2O_3$. Both gels (low and high-alumina content) presented a monomodal particle size distribution. Low-alumina gel (silica rich) presented lower particle size due to the fact that the precursor used in the sol-gel process (TEOS) can lead to the formation of colloidal silica when a diphasic gel is generated. This was later confirmed by the presence of an intense peak of cristobalite at the XRD patterns.

The XRD patterns obtained by annealing the gel confirm an incipient formation of mullite as temperatures as low as 1000°C (Figure 3).[30,31] Interestingly, the formation of mullite after annealing at 1000°C for 10 hours seems to be more pronounced for the high-alumina composition, which comprises also traces of crystalline alumina.[32] After fast heating to 1500°C followed by annealing for 10 hours, however, both compositions contain not only mullite but also alumina (delta and alfa) and silica (cristobalite),[33] the latter giving a strong signal.

The XRD patterns of the mullite inverse opal photonic crystals are presented in Figure 4 for (a) alumina-poor mullite and (b) alumina-rich mullite composition. Thereby, it has to be noted first that—although a low inclination measurement was performed—here the sample holder still contributes to the diffraction patterns due to the low thickness and high porosity of the inverse opal photonic structures investigated.[34] As consequence, there are strong peaks related to the aluminum sample holder (see Figure S1). Peaks related to $\delta$-$Al_2O_3$ and $\alpha$-$Al_2O_3$ were also identified, more pronounced in case of the low-alumina composition as shown in Figure 4A.

At 1200°C, the inverse opal photonic structures presented a considerable amount of small but detectable mullite grains; at 1400°C, all peaks associated with mullite are identified. Transformation of tetragonal mullite to orthorhombic mullite is usually observed in temperatures over 1400°C.[35,36] It has to be noted that, although the alumina-rich composition presented a peak typical of cristobalite,[37] the intensity of the peak is relatively small when compared with the low-alumina gel. Moreover, this composition shows a small peak at 1200°C and a larger one at

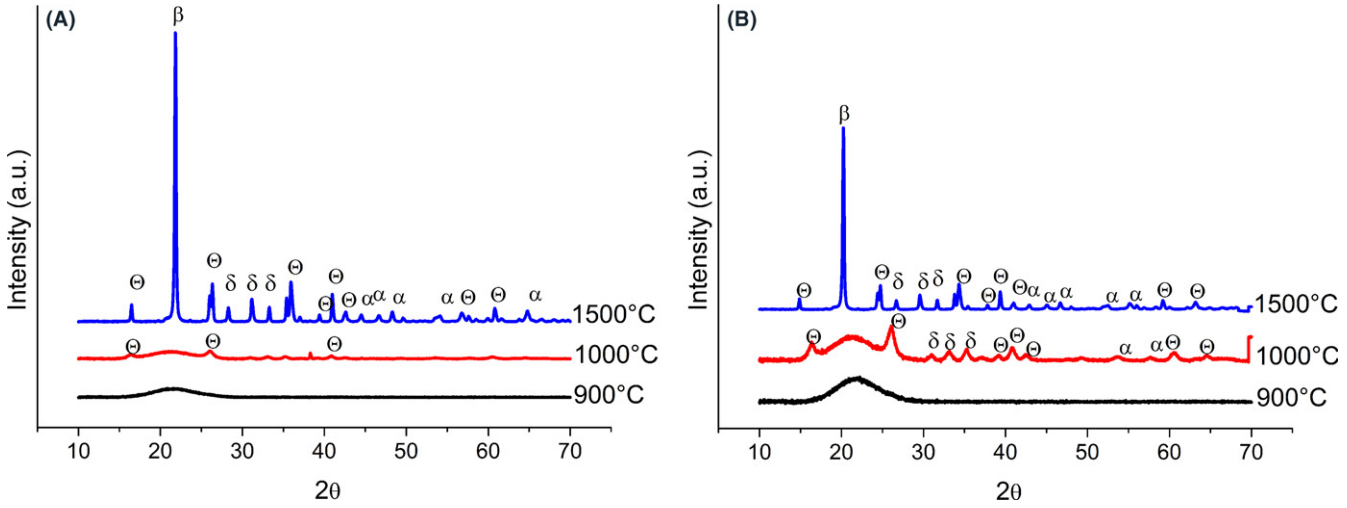


**FIGURE 3** XRD patterns of mullite inverse opal photonic crystals after calcination in air for 10 hours at 900, 1000 or 1500°C of: (A) low-alumina content sol-gel; (B) high-alumina content sol-gel. Mullite peaks (JCPDS card nr. 15-776, JCPDS card nr. 84-1205) are represented by θ, cristobalite (JCPDS card nr. 27-605) by $\beta$, $\alpha$-alumina (JCPDS card nr. 88-0826) by $\alpha$, and $\delta$-alumina (JCPDS card nr. 46-1131) by $\delta$

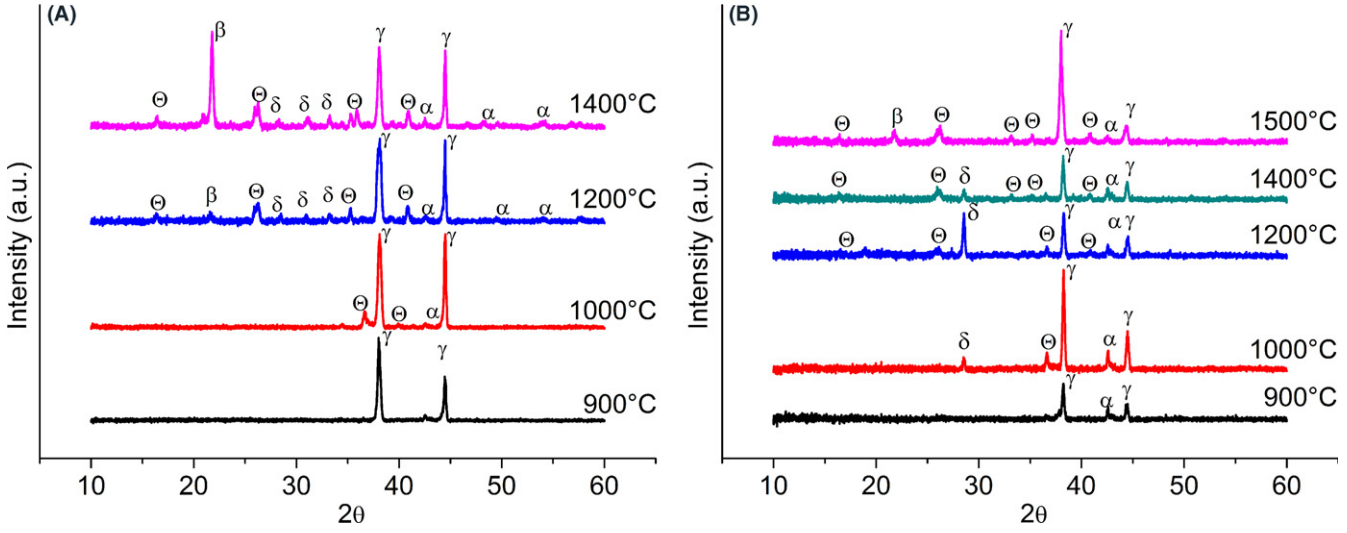


**FIGURE 4** XRD (GI) patterns of mullite inverse opal photonic crystals after calcination in air at 900, 1000, 1200°C for 1 hour, at 1400°C for 4 hours, or at 1500°C for 8 hours of: (A) low-alumina content sol-gel; (B) high-alumina content sol-gel. Mullite peaks (JCPDS card nr. 15-776, JCPDS card nr. 84-1205) are represented by θ, cristobalite (JCPDS card nr. 27-605) by $\beta$, $\alpha$-alumina (JCPDS card nr. 88-0826) by $\alpha$, $\delta$-alumina (JCPDS card nr. 46-1131) by $\delta$ and aluminum sample holder by $\gamma$

1400°C. The latter one most probably corresponds to crystallization and grain growth at higher temperatures.

## 3.1 | Microstructure evolution and stability

Packing of the PS spheres into 3D arrangement with FCC structure[1,2] was successful for both routes of template synthesis, vertical convective self-assembly as well as drop cast (Figure 5). Both direct photonic crystals show a high organized structure with only very few local distortions.

The SEM micrographs presented in Figure 6 show the inverse opal photonic crystals with interconnected macropores.[38] The solid skeleton formed from filling the interstitial space is apparently more stable in the photonic crystals obtained by drop casting (Figure 6A), when compared with the photonic crystals obtained through self-assembly (Figure 6B).[16]

According to the results shown in Table 1, it was possible to notice a trend related to the diameter and percentage area of pores to be decreasing after heat treatment. Conversely, the

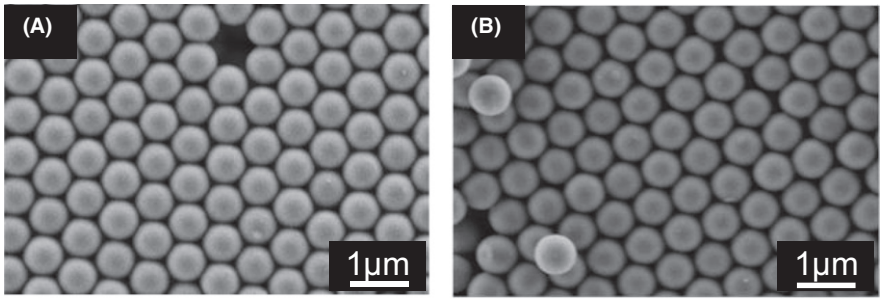


**FIGURE 5** SEM micrograph of PS direct photonic crystals obtained through: (A) self-assembly; (B) drop casting

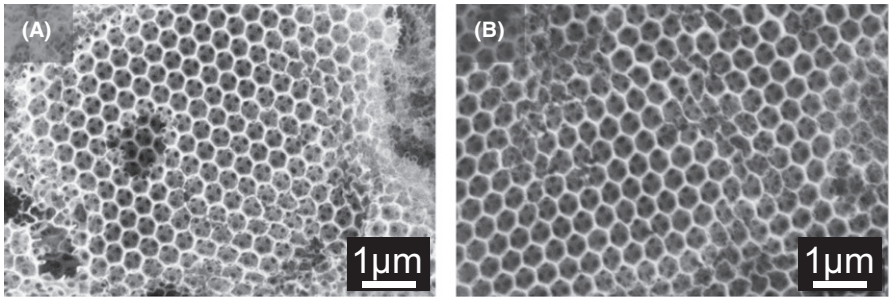


**FIGURE 6** SEM images of mullite inverse opal photonic crystals after burnout of PS spheres at 500°C of: (A) low-alumina sol-gel; (B) high-alumina sol-gel

**TABLE 1** Microstructure analysis by digital image processing of PS direct photonic crystals and mullite inverse opal photonic crystals before and after heat treatment

| **PS direct photonic crystals** | **Ø** | ***T* (°C)** | ***s**** **(μm)** | ***A*$_s$* (%)** | ***d*$_p$* (μm)** | ***A*$_p$* (%)** |
|---|---|---|---|---|---|---|
| Obtained by self-assembly | 0.983 | 25 | 0.054 ± 0.005 | 31.32 | 0.71 ± 0.01 | 68.68 |
| Obtained by drop casting | 0.971 | 25 | 0.060 ± 0.003 | 33.57 | 0.67 ± 0.02 | 66.43 |
| **Mullite inverse photonic crystals** | **Ø** | ***T* (°C)** | ***s**** **(μm)** | ***A*$_s$**** **(%)** | ***d*$_p$****(μm)** | ***A*$_p$**** **(%)** |
| Infiltrated with low-alumina content gel (74 wt.% $Al_2O_3$. 26 wt.% $SiO_2$) | 0.954 | 500 | 0.06 ± 0.01 | 32.88 | 0.50 ± 0.02 | 67.12 |
| | 0.962 | 900 | 0.08 ± 0.01 | 33.99 | 0.45 ± 0.02 | 66.01 |
| | 0.952 | 1000 | 0.10 ± 0.01 | 35.14 | 0.42 ± 0.02 | 64.86 |
| | 0.947 | 1200 | 0.11 ± 0.02 | 39.26 | 0.42 ± 0.02 | 60.74 |
| | 0.913 | 1400 | 0.12 ± 0.02 | 42.32 | 0.38 ± 0.03 | 57.68 |
| | — | 1500 | — | — | — | — |
| Infiltrated with high-alumina content gel (80 wt.% $Al_2O_3$. 20 wt.% $SiO_2$) | 0.967 | 500 | 0.08 ± 0.01 | 35.27 | 0.49 ± 0.02 | 64.73 |
| | 0.948 | 900 | 0.09 ± 0.02 | 37.10 | 0.44 ± 0.02 | 62.90 |
| | 0.954 | 1000 | 0.12 ± 0.02 | 38.59 | 0.41 ± 0.02 | 61.41 |
| | 0.938 | 1200 | 0.13 ± 0.02 | 39.88 | 0.40 ± 0.03 | 60.12 |
| | 0.911 | 1400 | 0.14 ± 0.01 | 42.92 | 0.37 ± 0.03 | 57.08 |
| | 0.870 | 1500 | 0.14 ± 0.02 | 44.77 | 0.31 ± 0.04 | 55.23 |

Ø, roundness (ideal sphere = 1); *s**, minimum distance (interstitial space) between PS microspheres; $A_s$*, percentage area of space between PS microspheres; *s***, minimum strut thickness after filling the interstitial space with mullite sol-gel; $A_s$**, percentage area of struts after filling with mullite sol-gel; $d_p$*, diameter of PS microspheres; $A_p$*, percentage area occupied by PS microspheres; $d_p$**, diameter of pores after thermal treatment; $A_p$**, percentage area occupied by pores after thermal treatment.

diameter and the percentage area of struts (thickness) is increasing. That corresponds to shrinkage of the pores after inversion of structure. The roundness of the PS microspheres, which was closer to 1 before heat treatment, deviates from the ideal sphere as the temperature of heat treatment gets higher, indicating a change in the original shape of pores. This is particularly noticed for the photonic crystals heat treated at 1500°C, due to the more pronounced sintering.

Strict significant changes in the structure of the mullite inverse opal photonic crystals heat treated at 900 and

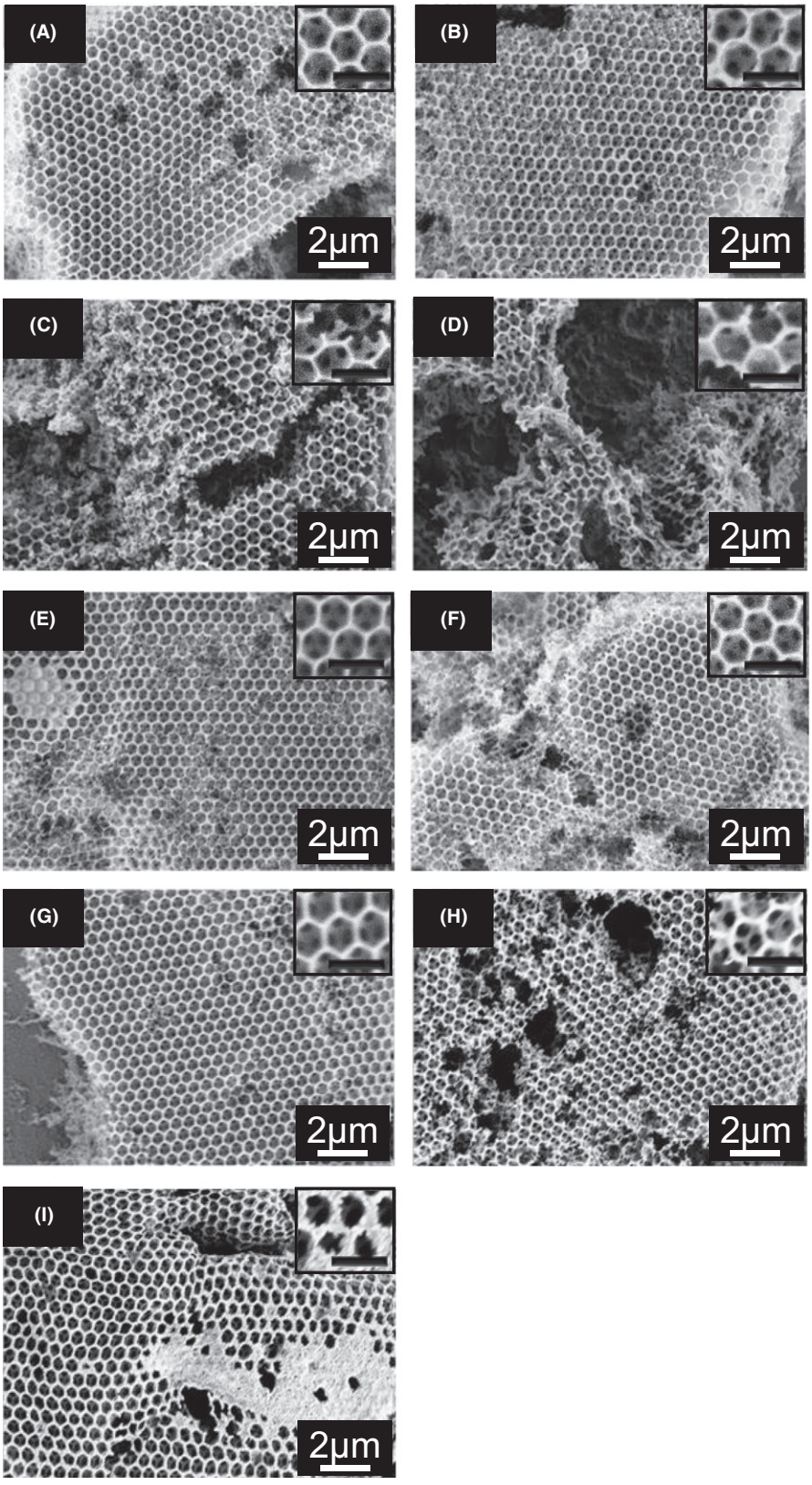


**FIGURE 7** SEM micrographs of mullite inverse opal photonic crystals (A-D) infiltrated with low-alumina sol-gel obtained through self-assembly and annealed in air, respectively, at: (A) 900°C, 1 hour; (B) 1000°C, 1 hour; (C) 1200°C, 1 hour; (D) 1400°C, 4 hours; and inverse opal photonic crystals (E-I) infiltrated with high-alumina sol-gel obtained through drop casting and annealed in air at: (E) 900°C, 1 hour; (F) 1000°C, 1 hour; (G) 1200°C, 1 hour; (H) 1400°C, 4 hours; (I) 1500°C, 8 hours

1000°C are not detectable (with the exception of a small shrinkage due to the heat treatment reported in Table 1), neither in case of alumina-poor composition nor in case of the alumina-rich composition. The ordering of the macropores still remained the same when compared to the state after burnout (Figure 7A and B). For the samples annealed at 1200°C for 1 hour and 1400°C for 4 hours, the inverse opal photonic crystals infiltrated with the low-alumina

composition showed a more pronounced change in the structure (Figure 7C-D), a behavior also observed for alumina inverse opal photonic crystals (higher shrinkage of structure).[39] A further increase in the annealing temperature to 1500°C resulted in a total collapse of the structural integrity of the low-alumina composition. Most probably, here the local composition can vary around the calculated nominal composition, resulting in local and transient presence of silica during heating up to the annealing temperature. This would cause constraints in the structure, which overcome the strength of the network causing thereby disintegration. This consideration is supported by the fact that in case of an alumina-rich composition the structure presented highly ordered macroporous even though the shape and size of pores were reduced at 1200 and 1400°C (Figure 7G-H), but even survive annealing at 1500°C for 8 hours. The main noticeable change in the structure of the alumina-rich photonic crystals heat treated at 1500°C is a more pronounced grain growth (Figure 7I) and reduction in pore size, as shown in Table 1). Nevertheless, the grain size is still submicrometric.

Moreover, it has to be noted that neither the low nor the high-alumina mullite composition resulted in structures, which exhibited a photonic bandgap after either burnout or annealing at moderate or high temperatures.[40] We attribute this to two effects acting simultaneously: (a) a low shell thickness and thereby less effective thickness of the structures synthesized here; (b) a slight distortion of the short range ordering during infiltration by spin coating. These distortions are most likely too small to be detected by SEM analysis, but already large enough to diminish the photonic band gap. Ongoing work using synchrotron nanotomography and ptychographic X-ray computed tomography to analyze the structural evolution as well as modeling of photonic performance will address the effect of structural distortions below the SEM detection limit.

## 4 | CONCLUSIONS

A new process for the synthesis of mullite inverse opal photonic crystals was reported. Direct photonic crystals were successfully prepared either by vertical convective self-assembly or by drop casting, the latter one being a much faster technique, that is, 30 minutes compared with at least 120 hours. A low mullite crystallization temperature of 1000°C was observed for the gels after XRD analysis, confirmed by the GI-XRD analysis of the 3D infiltrated inverse opal photonic structures.

Regardless the phase segregation presented by both gels, the inverse opal mullite photonic crystals have demonstrated high thermal stability, particularly in case of an alumina-rich composition. In this case, the porosity remained ordered, but with noticeable pore shape change, since the roundness value for samples heat treated at 900°C were closer to the ideal sphere (0.948), while the samples heat treated at 1500°C was not (0.870). Moreover, pore size decreased due to shrinkage of inverse structures after heat treatment (at 500°C to 0.490 μm, and at 1500°C to 0.308 μm). The inverse opal photonic crystals did not show a photonic bandgap but still presented structure stability at high temperatures (up to 1500°C), which enables their application as a refractory material.

## ACKNOWLEDGMENTS

The authors gratefully acknowledge financial support from the German Research Foundation (DFG) via SFB 986, project C5. P. Bueno is particularly thankful to the agencies CAPES (Brazil) and DAAD (Germany) for supporting her research stay in Hamburg. The sol-gel, PS direct photonic crystals, and mullite inverse opal photonic crystals characterization was carried by P. Bueno. All authors contributed to result analysis and discussion, as well as manuscript preparation and have given approval to its final version.

## ORCID

*Kaline Pagnan Furlan* http://orcid.org/0000-0003-4032-2795
*Rolf Janssen* http://orcid.org/0000-0001-7054-0510

## REFERENCES

1. Kubrin R, do Rosário JJ, Lee HS, Mohanty S, Subrahmanyam RP, Smirnova I, et al. Vertical convective co-assembly of refractory YSZ inverse opals from crystalline nanoparticles. ACS Appl Mater Interfaces. 2013;24(5):13146–52.
2. Liu H, Liu T, Dong X, Lv Y, Zhu Z. A novel fabrication of $SnO_2$ graphene oxide core/shell structures with enhanced visible photocatalytic activity. Mater Lett. 2014;126:36–8.
3. Pasquarelli RM, Lee HS, Kubrin R, Zierold R, Petrov AY, Nielsch K, et al. Enhanced structural and phase stability of titania inverse opals. J Eur Ceram Soc. 2015;35(11):3103–9.
4. Rudisill SG, Wang Z, Stein A. Maintaining the structure of templated porous materials for reactive and high-temperature applications. Langmuir. 2012;28(19):7310–24.
5. Arpin KA, Losego MD, Cloud AN, Ning H, Mallek J, Sergeant NP, et al. Three-dimensional self-assembled photonic crystals with high temperature stability for thermal emission modification. Nat Commun. 2013;4:1–8.
6. Checoury X, Enoch S, López C, Blanco A. Stacking patterns in self-assembly opal photonic crystals. Appl Phys Lett. 2007;90(16):161131.
7. Armstrong E, O'Dwyer C. Artificial opal photonic crystals and inverse opal structures fundamentals and applications from optics to energy storage. J Mater Chem C. 2015;3(24):6109–43.
8. Castañeda-Uribe OA, Méndez-Pinzón HA, Salcedo-Reyes JC, Pedroza-Rodríguez MA, Méndez-Pinzón HA. Fabrication and

optical characterization of a high-quality FCC-opal-based photonic crystals grown by the vertical convective self-assembly method. Universitas Scientiarum. 2010;15(2):150–8.
9. Jiang P, Bertone JF, Hwang KS, Colvin VL. Single-crystals colloidal multilayers of controlled thickness. Chem Mater. 1999;11 (8):2132–40.
10. Jiang P, McFarland MJ. Large-scale fabrication of wafer-size colloidal crystals, macroporous polymers and nanocomposites by spin-coating. J Am Chem Soc. 2004;126(42):13778–86.
11. Mihi A, Mígues H, Ocaña M. Oriented colloidal-crystals thin films by spin-coating microspheres dispersed in volatile media. Adv Mater. 2006;18(17):2244–9.
12. Yu J, Yan Q, Shen D. Co-self-assembly of binary colloidal crystals at the air water interface. ACS Appl Mater Interfaces. 2010;2 (7):1922–6.
13. do Rosário JJ, Dyachenko PN, Kubrin R, Pasquarelli RM, Petrov AY, Eich M, et al. Facile deposition of YSZ- inverse photonic glass films. ACS Appl Mater Interfaces. 2014;15(6):12335–45.
14. Kubrin R, Lee HS, Zierold R, Petrov AY, Janssen R, Nielsch K, et al. Stacking of ceramic inverse opals with different lattice constants. J Am Ceram Soc. 2012;95(7):2226–35.
15. Choy KL. Chemical vapour deposition of coatings. Prog Mater Sci. 2003;48(2):51–170.
16. Holland BT, Blanford CF, Stein A. Synthesis of macroporous minerals with highly ordered three-dimensional arrays of spheroidal voids. Science. 1998;281(5376):538–40.
17. Troczynski T, Yang Q, John G. Post-deposition treatment of zirconia thermal barrier coatings using Sol-Gel alumina. J Therm Spray Technol. 1999;8(02):229–34.
18. Viazzi C, Bonino JP, Ansart F. Synthesis by sol-gel route and characterization of Yttria Stabilized Zirconia coatings for thermal barrier applications. Surf Coat Technol. 2006;201(07):3889–993.
19. Weijje L, Zou B, Zhao J, Cui H. Optimizing sol–gel infiltration for the fabrication of high-quality titania inverse opal and its photocatalytic activity. Thin Solid Films. 2010;518(17):4923–7.
20. Taktak S, Baspinar MS. Wear and friction behaviour of alumina/ mullite composite by sol–gel infiltration technique. Mater Des. 2005;26(5):459–64.
21. de Sola ER, Estevan F, Torres FJ, Alarcon J. Effect of thermal treatment on the structural evolution of 3:2 and 2:1 mullite monophasic gels. J Non-Cryst Solids. 2005;351(14–15):1202–9.
22. Dokko PC, Pask JA, Mazdiyasni KS. High temperature mechanical properties of mullite under compression. J Am Ceram Soc. 1977;60(3–4):150–5.
23. Aksay A, Dabbs DM, Sarikaya M. Mullite for structural, electronic, and optical applications. J Am Ceram Soc. 1991;74 (10):2343–58.
24. Cassidy DJ, Bartlett JR, Woolfrey JL, Ben-Nissan B. The effect of precursor chemistry on the crystallization and densification of sol-gel derived mullite gels and powders. J Sol-Gel Sci Technol. 1997;10(1):19–30.
25. Furlan KP, Krekeler T, Ritter M, Blick R, Schneider GA, Nielsch K, et al. Low-temperature mullite formation in ternary oxide coatings deposited by ALD for high-temperature applications. ACS Adv Mater Interfaces. 2017;4(23):1–8.
26. Hoffman DW, Roy RR, Komarneni S. Diphasic xerogels, a new class of materials: phases in the system $Al_2O_3$–$SiO_2$. J Am Ceram Soc. 1984;67:478–81.
27. Fukuoka M, Onoda Y, Inoue S, Wada K, Nukui A, Makishima A. The role of precursors in the structure of $SiO_2$–$Al_2O_3$ sols and gels by the sol-gel process. J Sol-Gel Sci Technol. 1993;1:47–56.
28. Okada K, Otsuka N. Characterization of the spinel phase from $SiO_2$–$A1_2O_3$ xerogels the formation process of mullite. J Am Ceram Soc. 1986;69(9):652–6.
29. Jaymes I, Douy A, Massiot D, Coutures P. Characterization of mono- and diphasic mullite precursor powders prepared by aqueous routes. 27Al and 29Si MAS-NMR spectroscopy investigations. J Mater Sci. 1996;31(17):4581–9.
30. Yoldas BE. Effect of ultrastructure on crystallization of mullite. J Mater Sci. 1992;27(24):6667–72.
31. Narendar Y, Messing GL. Mechanisms of phase separation in gel-based synthesis of multicomponent metal oxides. Catal Today. 1997;35(3):247–68.
32. Tan H, Ding Y, Yang J. Synthesis and characterization of rich silica mullite fibers by sol-gel method using aluminum lactate and silica sol. Adv Compos Mater. 2011;20(5):477–86.
33. Schneider H, Saruhan B, Voll D, Merwin L, Sebald A. Mullite precursor phases. J Eur Ceram Soc. 1993;11(1):87–94.
34. Chang SL. Thin-film characterization by grazing incidence X-ray diffraction and multiple beam interference. J Phys Chem Solids. 2001;62(9–10):1765–75.
35. Hyatt MJ, Bansal NP. Phase transformations in xerogels of mullite composition. J Mater Sci. 1990;25(6):2815–21.
36. Sundaresan S, Aksay IA. Mullitization of diphasic aluminosilicate gels. J Am Ceram Soc. 1991;74(10):2388–92.
37. Padmaja P, Anilkumar GM, Mukundan P, Aruldhas G, Warrier KGK. Characterization of stoichiometric sol–gel mullite by Fourier transform infrared spectroscopy. Int J Inorg Mater. 2001;3 (7):693–8.
38. Wijnhoven JEGJ, Bechger L, Vos WL. Fabrication and characterization of large macroporous photonic crystals in titania. Chem Mater. 2001;13(12):4486–99.
39. Sokolov S, Bell D, Stein A. Preparation and characterization of macroporous alfa-alumina. J Am Ceram Soc. 2003;86(9):1481–6.
40. Furlan KP, Pasquarelli RM, Krekeler T, Ritter M, Zierold R, Nielsch K, et al. Highly porous α-$Al_2O_3$ ceramics obtained by sintering atomic layer deposited inverse opals. Ceram Int. 2017;43(14):11260–4.

## SUPPORTING INFORMATION

Additional supporting information may be found online in the Supporting Information section at the end of the article.

**How to cite this article:** Bueno P, Pagnan Furlan K, Hotza D, Janssen R. High-temperature stable inverse opal photonic crystals via mullite-sol-gel infiltration of direct photonic crystals. *J Am Ceram Soc*. 2018;00:1–9. https://doi.org/10.1111/jace.16012